Обзор ArXiv/astro-ph, 2 марта 2022 года

От Сильченко О.К.

Costantin et al. 2021: Статья 1

CrossMark

A Duality in the Origin of Bulges and Spheroidal Galaxies

Luca Costantin[1], Pablo G. Pérez-González[1], Jairo Méndez-Abreu[2,3,4,5], Marc Huertas-Company[2,3,6], Paola Dimauro[7], Belén Alcalde-Pampliega[8], Fernando Buitrago[9], Daniel Ceverino[10,11], Emanuele Daddi[12], Helena Domínguez-Sánchez[13,14], Néstor Espino-Briones[15], Antonio Hernán-Caballero[16], Anton M. Koekemoer[17], and Giulia Rodighiero[18]

[1] Centro de Astrobiología (CSIC-INTA), Ctra de Ajalvir km 4, Torrejón de Ardoz, E-28850, Madrid, Spain; lcostantin@cab.inta-csic.es
[2] Instituto de Astrofísica de Canarias, E-38200, La Laguna, Tenerife, Spain
[3] Departamento de Astrofísica, Universidad de La Laguna, E-38205, La Laguna, Tenerife, Spain
[4] Dpto. de Física y del Cosmos, Campus de Fuentenueva, Edificio Mecenas, Universidad de Granada, E-18071, Granada, Spain
[5] Instituto Carlos I de Física Teórica y Computacional, Facultad de Ciencias, E-18071, Granada, Spain
[6] LERMA, Observatoire de Paris, CNRS, PSL, Université de Paris, France
[7] Observatório Nacional, Rua General José Cristino, 77, São Cristóvão, 20921-400, Rio de Janeiro, Brazil
[8] European Southern Observatory (ESO), Alonso de Córdova 3107, Vitacura, Casilla 19001, Santiago de Chile, Chile
[9] Instituto de Astrofísica e Ciências do Espaço, Universidade de Lisboa, Tapada da Ajuda, 1349-018, Lisbon, Portugal
[10] Universidad Autonoma de Madrid, Ciudad Universitaria de Cantoblanco, E-28049, Madrid, Spain
[11] CIAFF, Facultad de Ciencias, Universidad Autonoma de Madrid, E-28049 Madrid, Spain
[12] AIM, CEA, CNRS, Université Paris-Saclay, Université Paris Diderot, Sorbonne Paris Cité, F-91191, Gif-sur-Yvette, France
[13] Institute of Space Sciences (ICE, CSIC), Campus UAB, Carrer de Magrans, E-08193, Barcelona, Spain
[14] Institut d'Estudis Espacials de Catalunya (IEEC), E-08034, Barcelona, Spain
[15] Departamento de Física de la Tierra y Astrofísica, Faultad de CC Físicas, Universidad Complutense de Madrid, E-28040, Madrid, Spain
[16] Centro de Estudios de Física del Cosmos de Aragón, Plaza San Juan 1, planta 2, E-44001, Teruel, Spain
[17] Space Telescope Science Institute, 3700 San Martin Drive, Baltimore, MD 21218, USA
[18] Department of Physics and Astronomy, University of Padova, Vicolo Osservatorio 3, I-35122, Padova, Italy

Received 2020 December 17; revised 2021 February 26; accepted 2021 March 15; published 2021 June 2

Выборка галактик

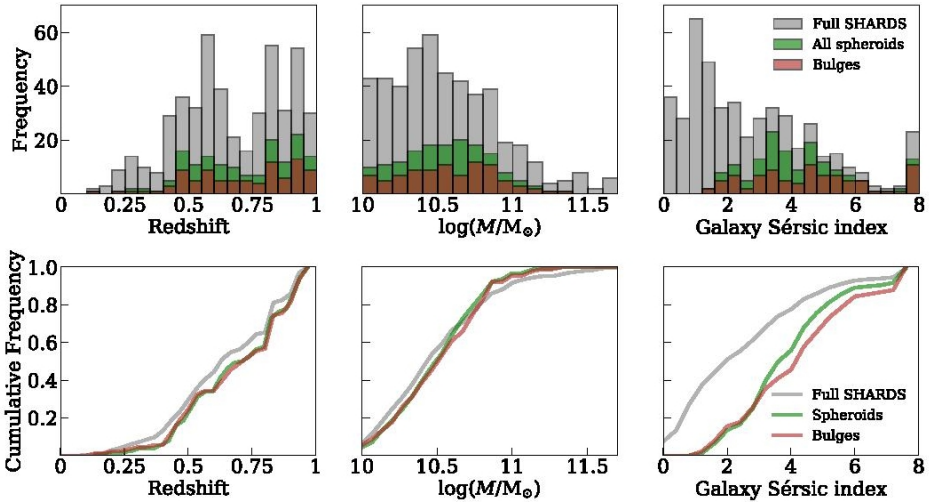

The final sample is composed of 156 galaxies, 65 pure spheroids, and 91 galaxies with a bulge and disk component, as presented in Figure 1 (green and red histograms). Ten more galaxies were discarded from the 166 galaxies analyzed because the 2D modeling of their individual SEDs provides no constraints for their stellar populations (see Sections 3.1.1 and 3.2). The representativeness of the final sample is checked by means of a Kolmogorov–Smirnov test, assuring that each subsample does not introduce any substantial bias in the $(z, M_\star)$ parameter space (p-value$_z > 10\%$, p-value$_{M_\star} > 30\%$). Moreover, it is worth nothing that our selection clearly discards galaxies modeled with low values of the Sérsic index ($n \lesssim 1.5$). This is mainly because we focus on the spheroidal component, partially due to our inclination threshold, but also because we checked the goodness of our selection for each individual galaxy, discarding unphysical or poorly constrained solutions.

Обзор SHARDS на GTC:
25 50-ти ангстремных фильтров

Для фотометрической декомпозиции привлекают данные HST

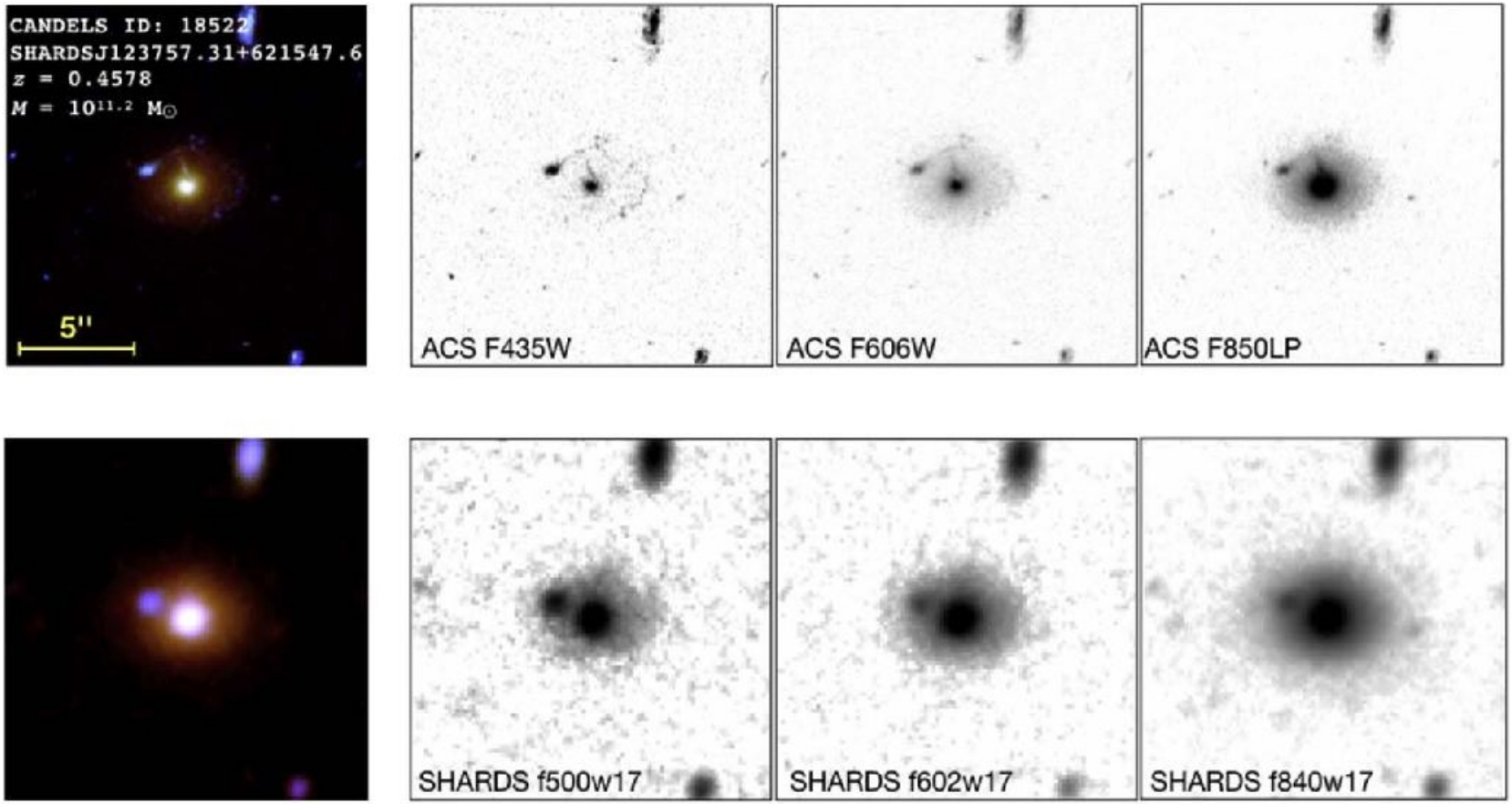

Figure 2. From left to right: postage RGB images for a typical galaxy in our sample (GDN 18522) and corresponding images in the three different filters: HST ACS F435W, F600W, and F850LP (top panels) and SHARDS f500w17, f602w17, and f840w17 (bottom panels). The galaxy is oriented north up, east to the left, and the field of view is 18×18 arcsec^2.

Пример очень хорошей декомпозиции

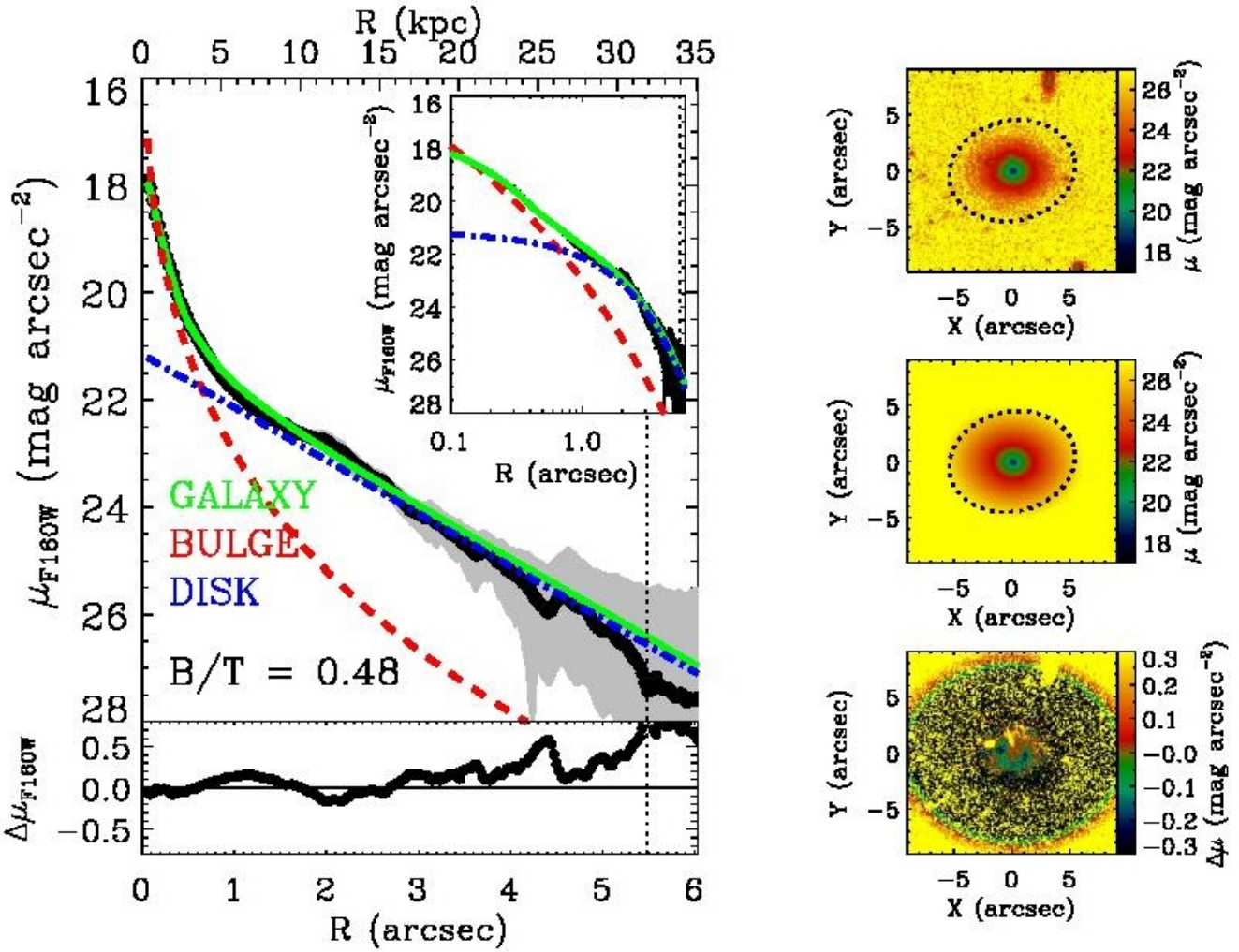

Для каждой галактики – SED балджа и диска

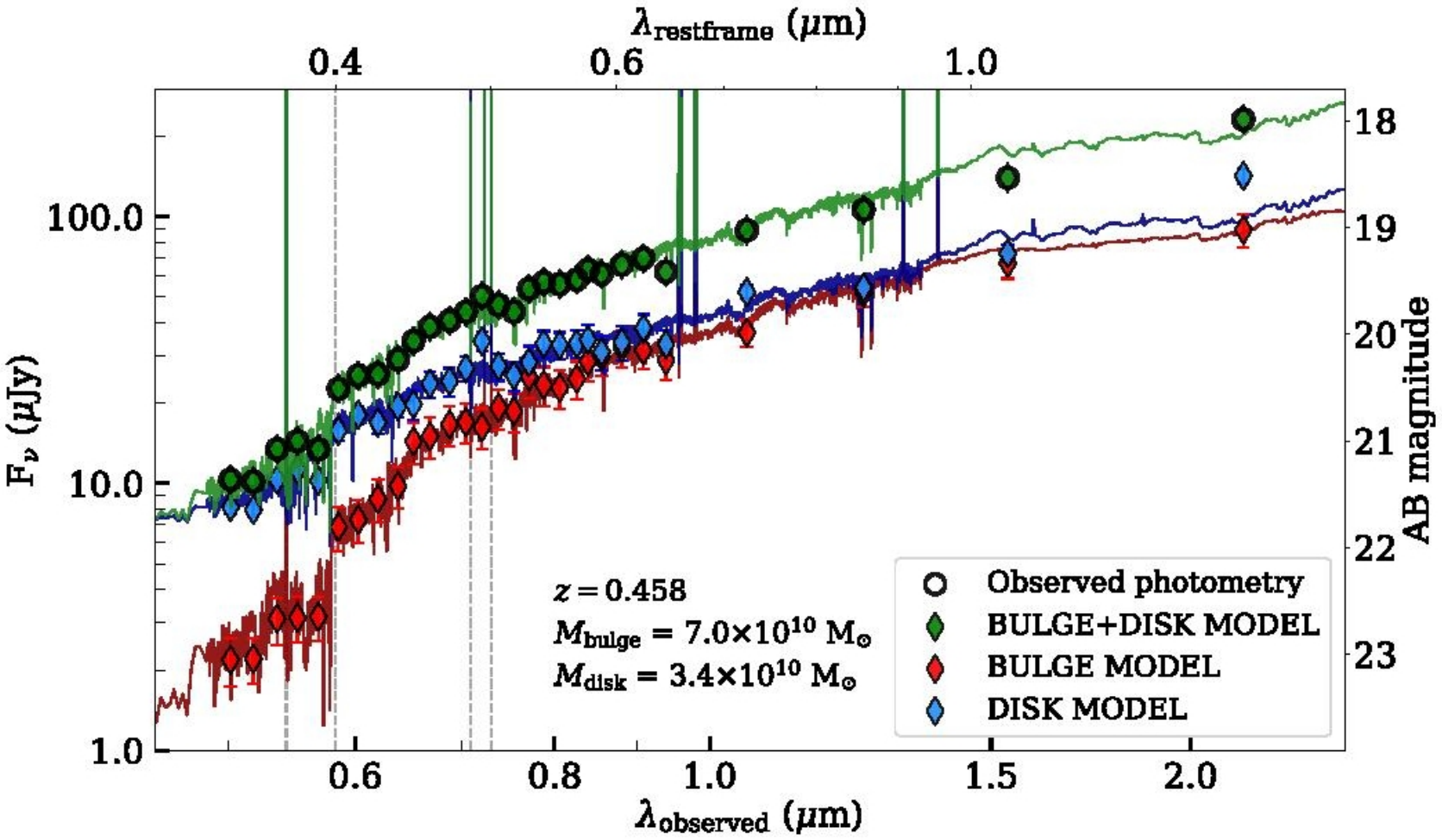

Бимодальность возрастов и эпох формирования сфероидов

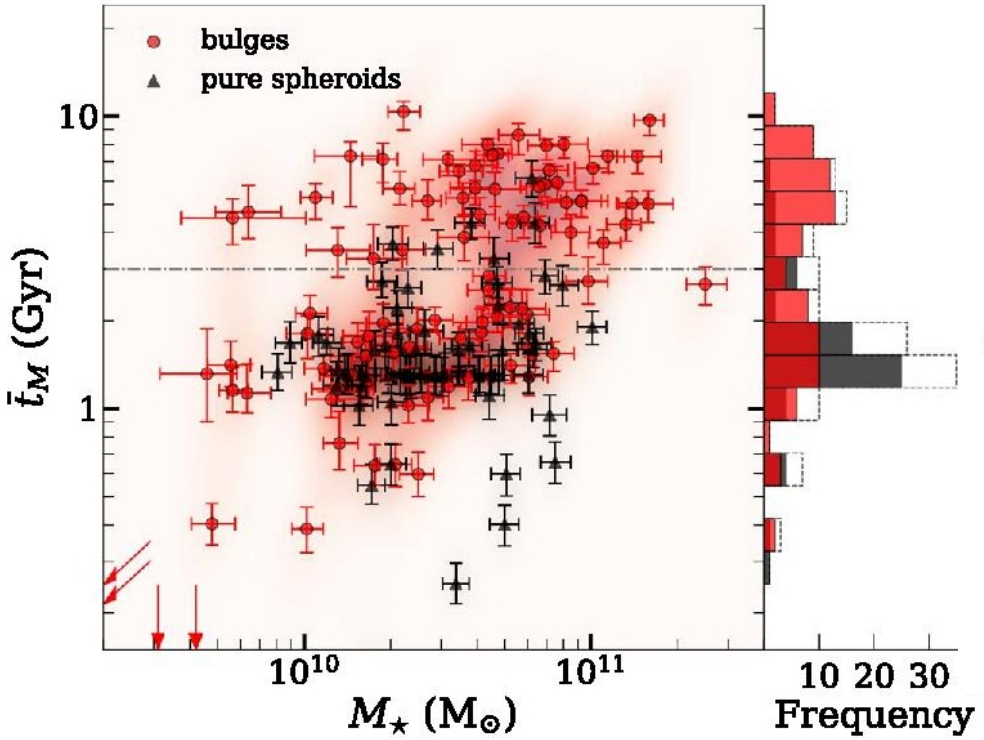

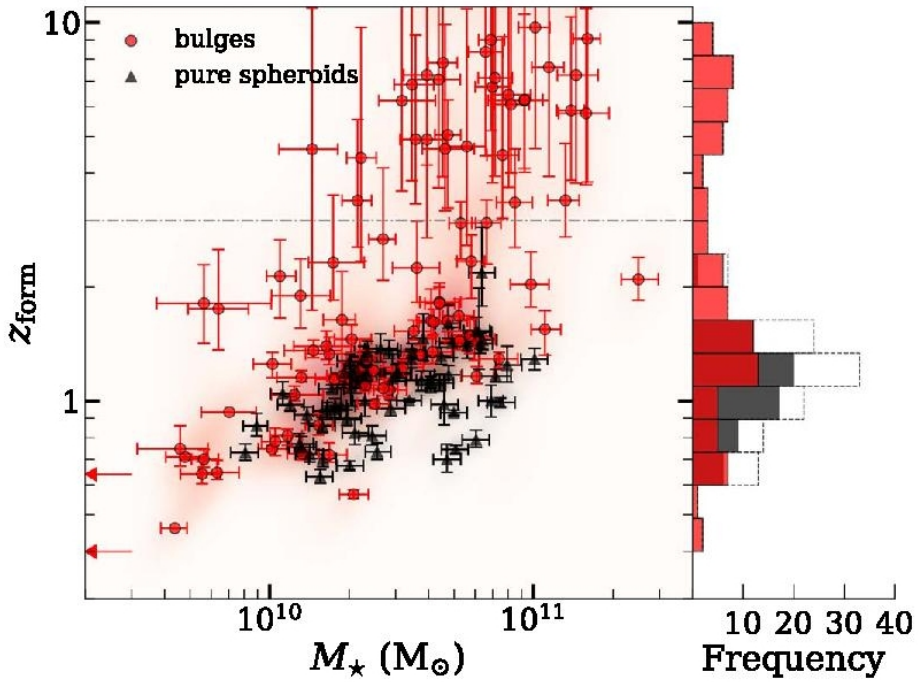

Быстрое формирование и тех, и других, но старые - плотнее

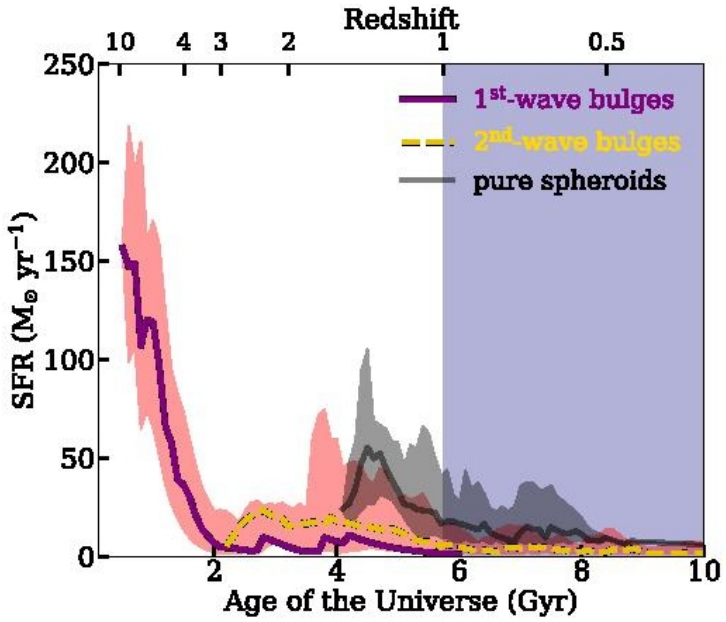

Figure 12. Averaged SFHs of the first-wave bulges (purple solid line), second-wave bulges (orange dashed line), and pure spheroids (black solid line). The red and black shaded curves represent the corresponding 16th–84th percentile interval. The blue shaded area indicates the redshift studied in this work.

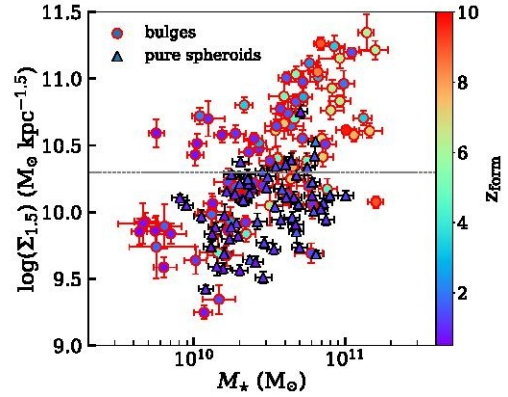

Figure 10. Mass surface density $MR_e^{-1.5}$ of bulges (circles) and pure spheroids (triangles) as a function of their mass, color-coded according to their formation redshift z_{form}. Errors are reported as the 16th–84th percentile interval. Systems are separated between compact and extended ones at $\log(\Sigma_{1.5}) = 10.3$ $M_\odot$ kpc$^{-1.5}$ (dashed gray horizontal line; Barro et al. 2013).

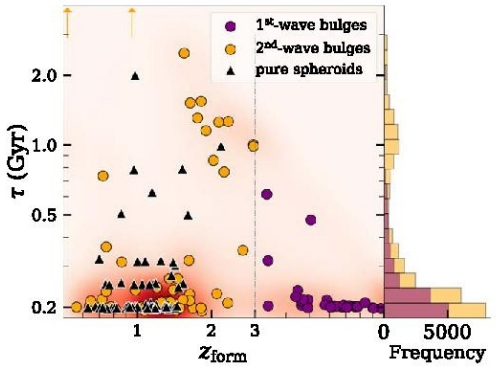

Figure 11. Distribution of timescales as a function of formation redshift for our bulges (first wave: purple circles; second wave: orange circles) and pure spheroids (black triangles). The red shaded region shows the density distribution of the 500 MC realizations for each bulge. The purple and orange histograms represent the frequency of the timescales for all the MC realizations of first- and second-wave bulges, respectively.

Сценарий для сфероидов

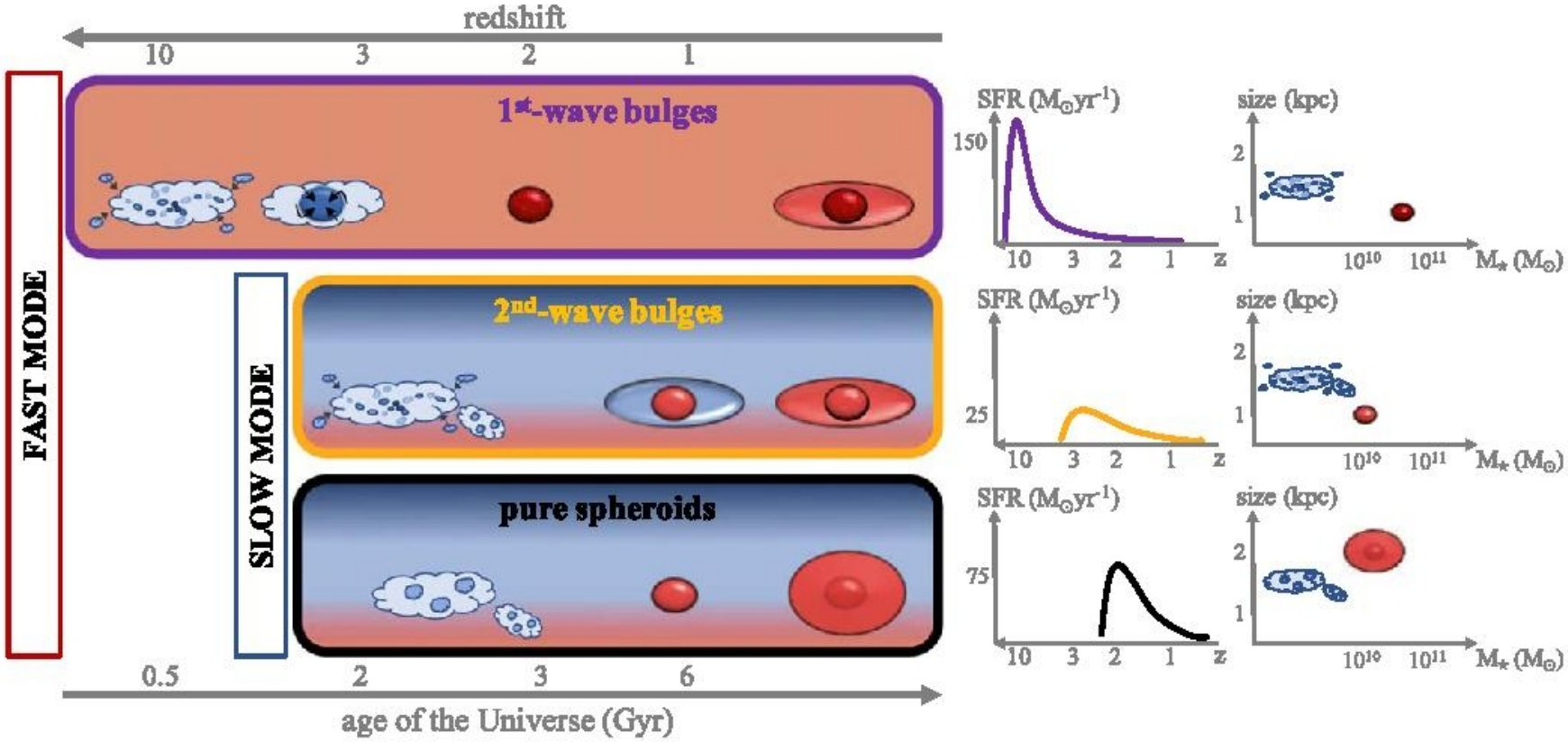

Table 2
Median Physical Properties of the Spheroidal Population at Redshift $0.14 < z \leqslant 1$

Type	$\log(M_*)$ ($M_\odot$)	$\tilde{t}_M$ (Gyr)	$z_{\rm form}$	τ (Myr)	R_e (kpc)	$\log(\Sigma_{1.5})$ ($M_\odot$ kpc$^{-1.5}$)
(1)	(2)	(3)	(4)	(5)	(6)	(7)
First-wave bulges	$10.8^{+0.2}_{-0.3}$	$6.5^{+1.5}_{-1.4}$	$6.2^{+1.5}_{-1.7}$	203^{+15}_{-3}	$1.3^{+0.8}_{-0.6}$	$10.6^{+0.4}_{-0.4}$
Second-wave bulges	$10.3^{+0.4}_{-0.5}$	$1.7^{+2.0}_{-0.8}$	$1.3^{+0.6}_{-0.6}$	213^{+790}_{-13}	$1.0^{+0.8}_{-0.4}$	$10.2^{+0.5}_{-0.4}$
Pure spheroids	$10.5^{+0.3}_{-0.2}$	$1.3^{+1.2}_{-0.2}$	$1.1^{+0.3}_{-0.3}$	201^{+114}_{-3}	$1.9^{+1.4}_{-0.6}$	$10.1^{+0.2}_{-0.3}$

Note. Column (1): spheroidal type. Column (2): stellar mass of each component. Column (3): mass-weighted age. Column (4): redshift of formation. Column (5): timescale of exponentially declined SFH. Column (6): effective radius. Column (7): mass surface density.

ArXiv: 2202.02332

From naked spheroids to disky galaxies: how do massive disk galaxies shape their morphology?

Luca Costantin [1,2] Pablo G. Pérez-González [1,3] Jairo Méndez-Abreu [4,5] Marc Huertas-Company [4,5,6]
Belén Alcalde Pampliega [7] Marc Balcells [8,4,5] Guillermo Barro [9] Daniel Ceverino [10,11]
Paola Dimauro [12] Helena Domínguez Sánchez [13,14] Néstor Espino-Briones [15] and
Anton M. Koekemoer [16]

[1] *Centro de Astrobiología (CSIC-INTA), Ctra de Ajalvir km 4, Torrejón de Ardoz, 28850, Madrid, Spain*
[2] *INAF - Osservatorio Astronomico di Brera, Via Brera 28, 20121, Milano, Italy*
[3] *Honorary professor, Departamento de Física de la Tierra y Astrofísica, Facultad de CC. Físicas, Universidad Complutense de Madrid, 28040 Madrid, Spain*
[4] *Instituto de Astrofísica de Canarias, 38200, La Laguna, Tenerife, Spain*
[5] *Departamento de Astrofísica, Universidad de La Laguna, 38205, La Laguna, Tenerife, Spain*
[6] *LERMA, Observatoire de Paris, CNRS, PSL, Université de Paris, France*
[7] *European Southern Observatory (ESO), Alonso de Córdova 3107, Vitacura, Casilla 19001, Santiago de Chile, Chile*
[8] *Isaac Newton Group of Telescopes, Apartado 321, 38700, Santa Cruz de La Palma, Islas Canarias, Spain*
[9] *Department of Physics, University of the Pacific, 3601 Pacific Ave., Stockton, CA 95211, USA*
[10] *Universidad Autonoma de Madrid, Ciudad Universitaria de Cantoblanco, 28049, Madrid, Spain*
[11] *CIAFF, Facultad de Ciencias, Universidad Autonoma de Madrid, 28049 Madrid, Spain*
[12] *Observatório Nacional, Rua General José Cristino, 77, São Cristóvão, 20921-400, Rio de Janeiro, Brazil*
[13] *Institute of Space Sciences (ICE, CSIC), Campus UAB, Carrer de Magrans, 08193, Barcelona, Spain*
[14] *Institut d'Estudis Espacials de Catalunya (IEEC), 08034, Barcelona, Spain*
[15] *Instituto Nacional de Astrofísica, Óptica y Electrónica, Luis E. Erro No. 1, Tonantzintla, 72840 Puebla, México*
[16] *Space Telescope Science Institute, 3700 San Martin Dr., Baltimore, MD 21218, USA*

По той же выборке и методике взялись за диски..

Выборка

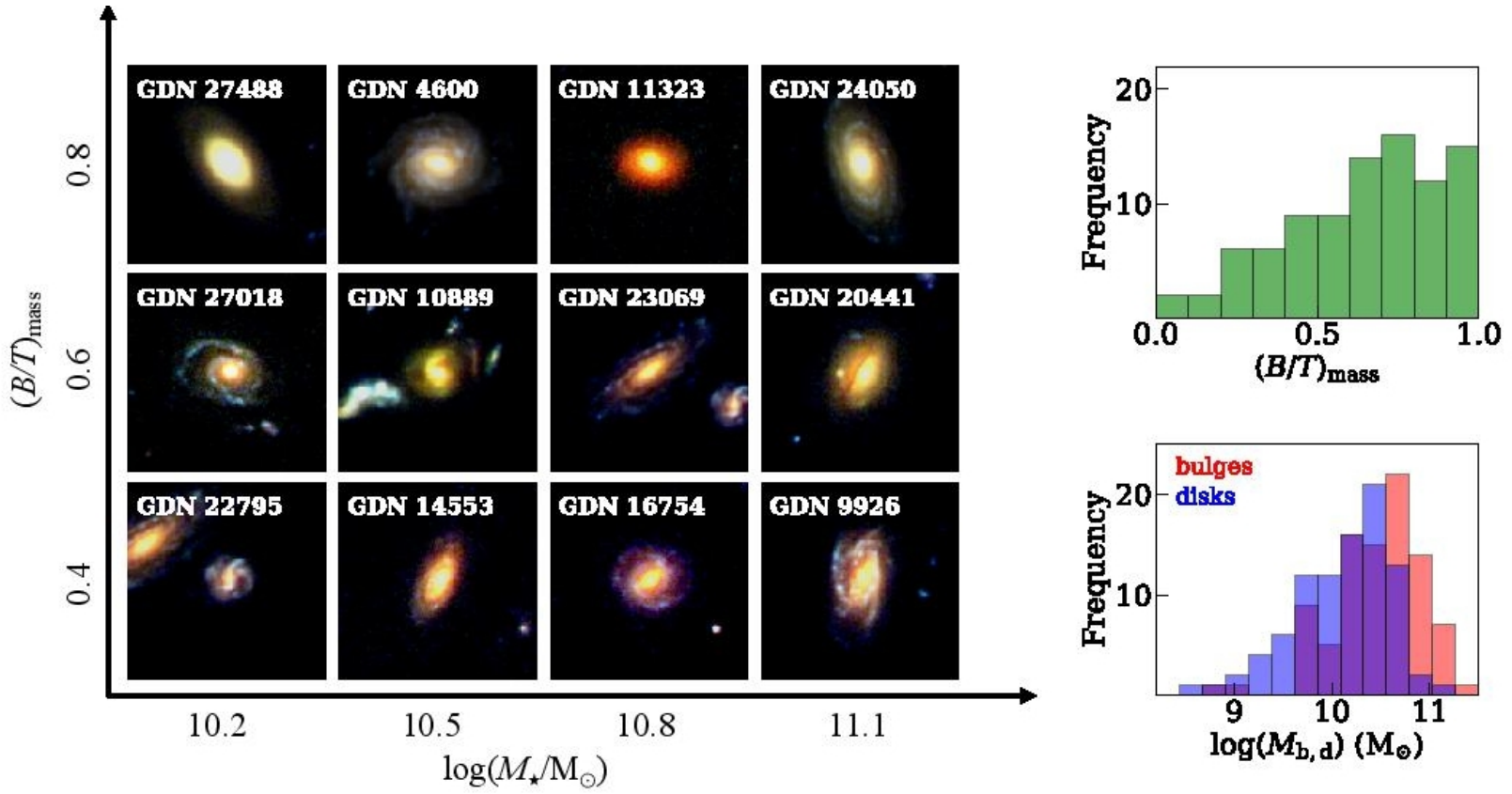

Figure 1. Left panel: Visual examples from the HST imaging (Koekemoer et al. 2011) of the diversity of morphologies of our galaxies as a function of their stellar mass and bulge-over-total mass ratio $(B/T)_{\rm mass}$. Right panels: Bulge-over-total mass ratio (green) and mass distributions of bulges (red) and disks (blue).

Результаты

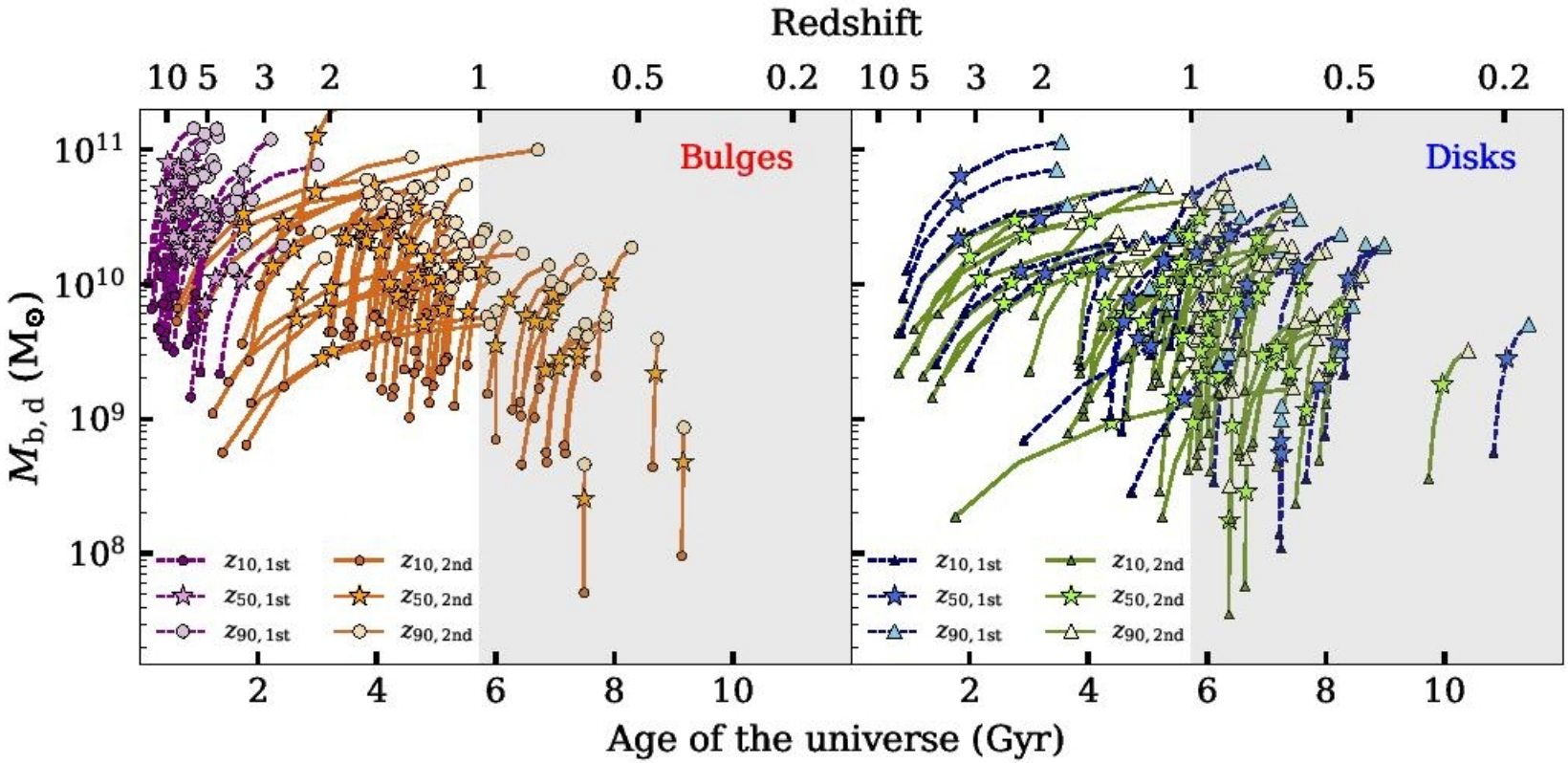

Figure 3. Mass assembly history of our bulges (left panel) and disks (right panel) as a function of the age of the universe. Bulges are separated between first-wave (purple dashed lines) and second-wave ones (orange solid lines). Disks are separated between those around first-wave bulges (blue dashed lines) and those around second-wave bulges (green solid lines). For each system we mark the instants when they build 10%, 50%, and 90% of the current stellar mass (from darker to lighter colors, from smaller to larger sizes). In particular, stars stand for z_{50}, i.e., the redshift when each system grows half of its current mass. The gray shaded regions stand for the redshift of observation.

Истории формирования

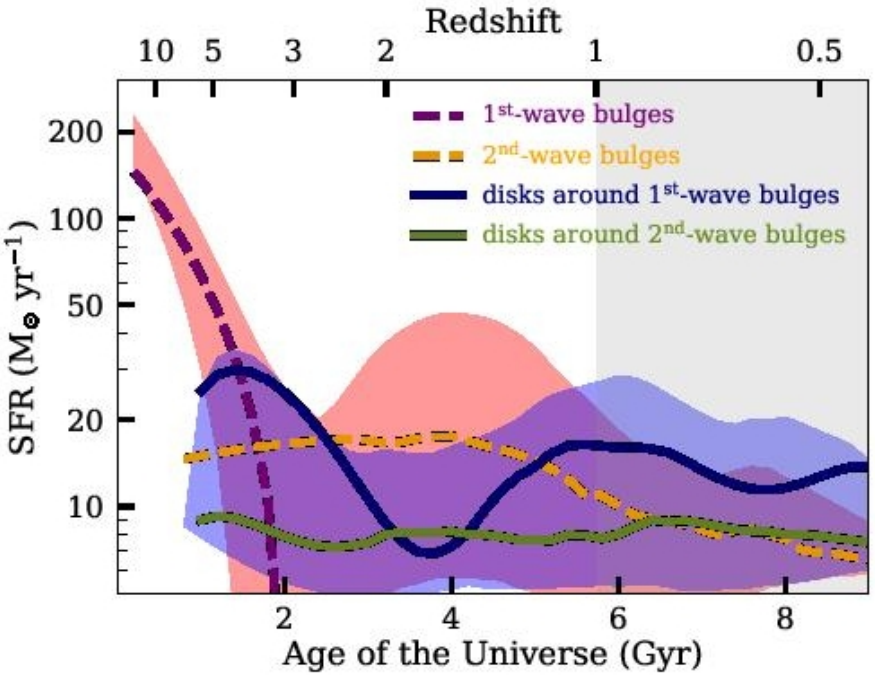

Figure 4. Averaged SFHs of the first-wave bulges (purple dashed line) and disks around them (blue solid line), compared with the one of second-wave bulges (orange dashed line) and disks around them (green solid line). The red and blue shaded curves represent the 16th–84th percentile interval computed from the scatter of the SFHs of bulges and disks, respectively. The gray shaded area indicates the redshift studied in this work.

Диски – все во вторую волну?

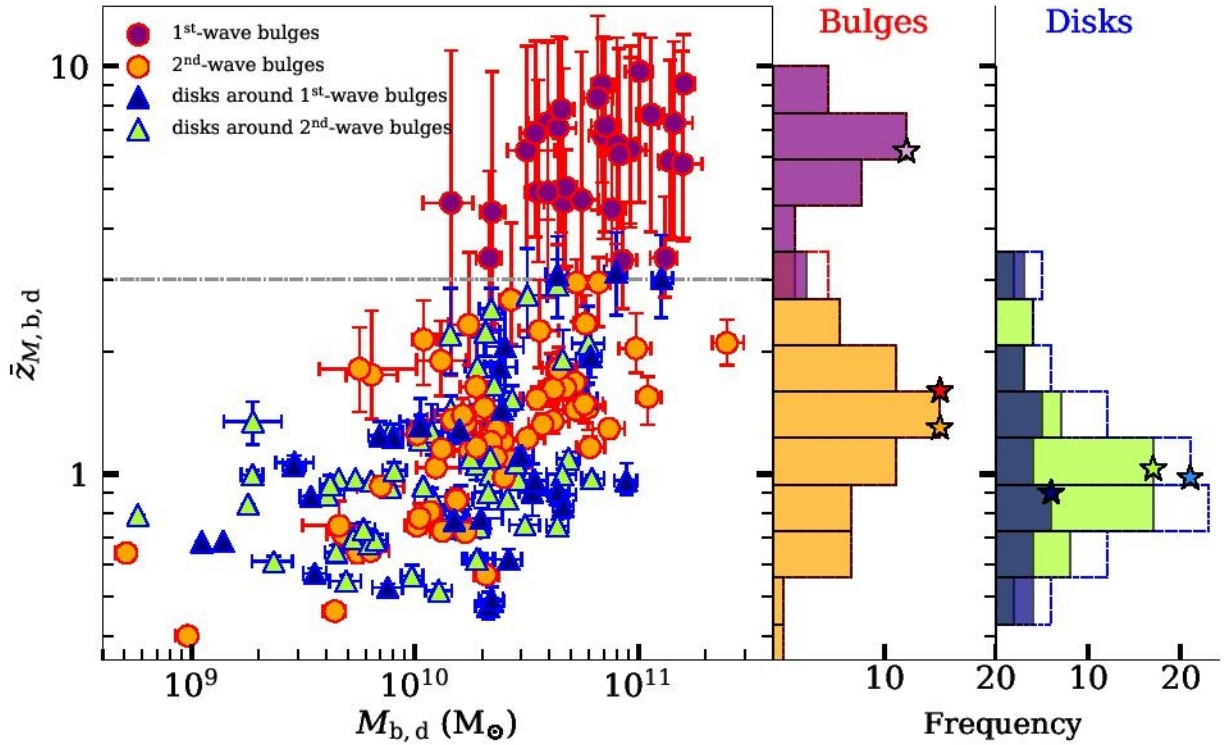

Figure 5. Mass-weighted formation redshift of bulges (dots) and disks (triangles) as a function of their stellar mass. Bulges and disks are separated in first-wave (purple and blue, respectively) and second-wave ones (orange and green, respectively). Errors are reported as 16th–84th percentile interval. The gray dash-dotted horizontal line marks $\bar{z}_M = 3$. The histograms represent the frequency of the mass-weighted formation redshifts of the bulge and disk populations, respectively. Purple and orange histograms stand for first and second-wave bulges, while the histogram with red dashed contour stands for the entire bulge population. Blue and green histograms stand for disks around first and second-wave bulges, while the histogram with

… причем во вторую волну – как до, так и после балджей

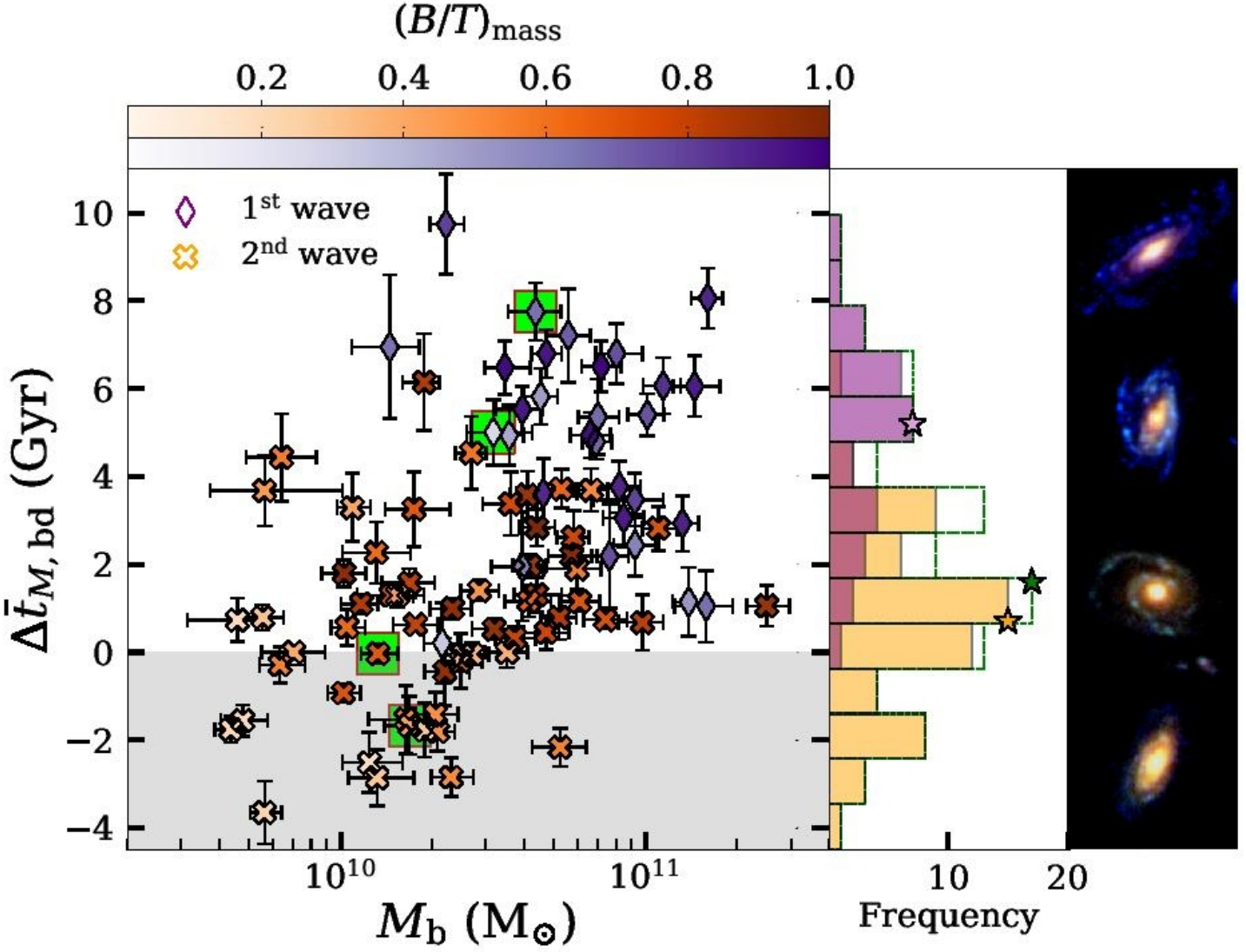

Поиски эволюционных корреляций…

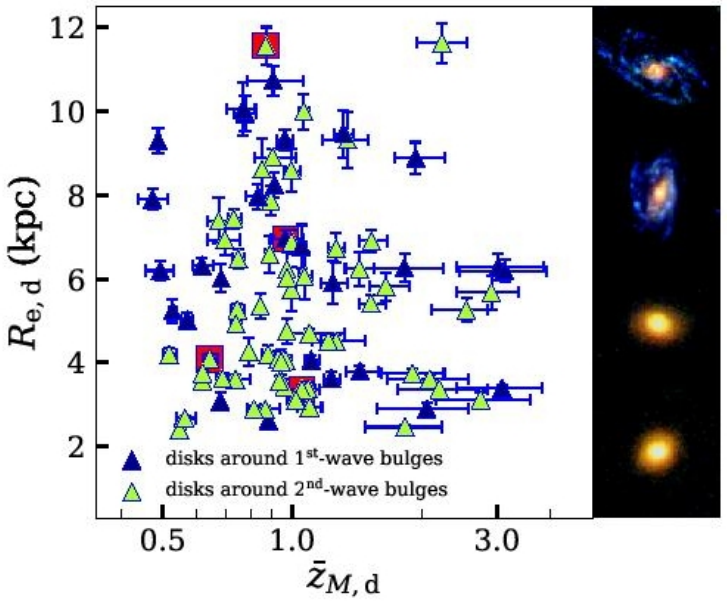

Figure 7. Size of disks as a function of their mass-weighted formation redshift. Disks around first and second-wave bulges are shown in blue and green, respectively. Errors are reported as the 16th–84th percentile interval. Red squares mark the four galaxies shown in RGB colors as an example (right panels).

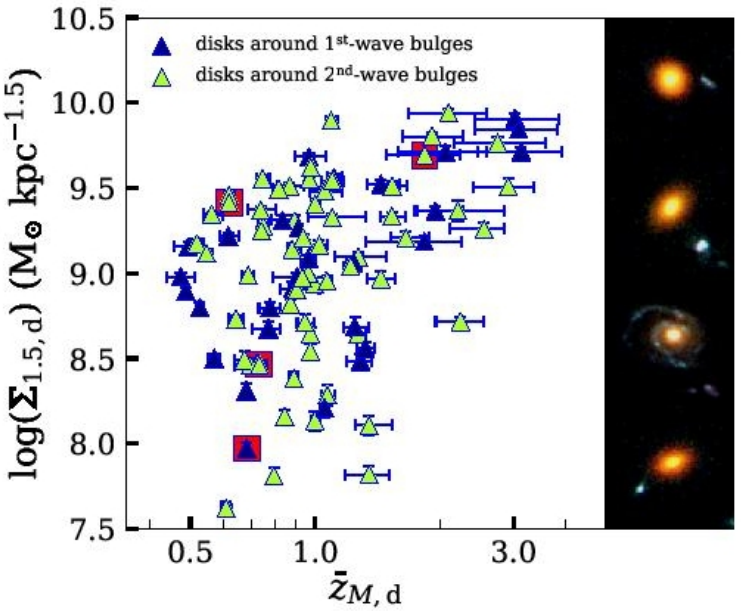

Figure 8. Mass surface density of disks as a function of their mass-weighted formation redshift. Disks around first and second-wave bulges are shown in blue and green, respectively. Errors are reported as 16th–84th percentile interval. Red squares mark the four galaxies shown in RGB colors as an example (right panels).

Связь со сценарием псевдобалджей – не просматривается

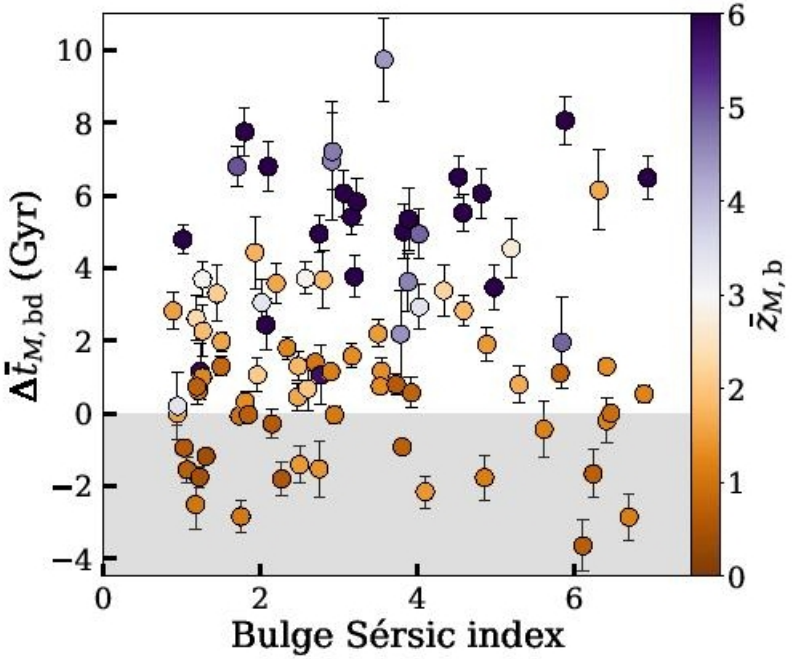

Figure 9. Age difference of bulges and disks as a function of the bulge Sérsic index, color-coded according to the bulge mass-weighted formation redshift. Errors are reported as 16th–84th percentile interval. The gray shaded region marks $\Delta\bar{t}_{M,\mathrm{bd}} < 0$.

Опять сценарий

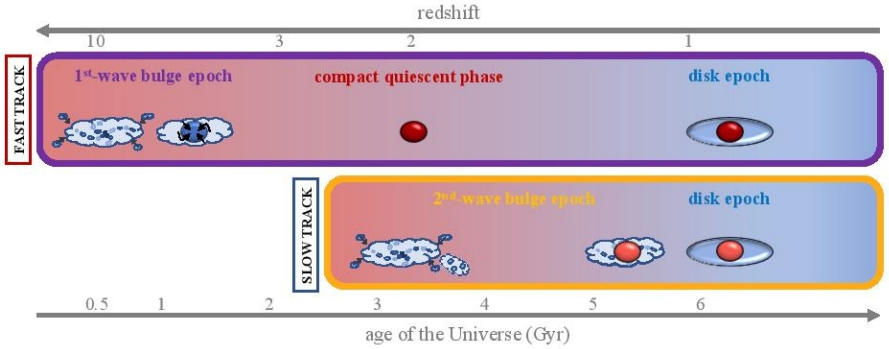

Figure 10. Illustration of the proposed scenario for the formation and morphological evolution of massive disk galaxies at redshift $0.14 < z \leq 1$. This cartoon complement the picture detailed in Paper I (Fig. 13), adding the information about the disk growth. The upper panel shows the evolution of fast-track systems. These galaxies build a compact spheroid at high redshift through an intense episode of star formation (first-wave bulge), evolve rapidly through a blue and red-nugget phase ($z \sim 1.5-3$), and grow an extended stellar disk by redshift $z \sim 1$. The lower panel shows the evolution of slow-track systems. In these galaxies there is a high level of (slow) co-evolution between the spheroidal (second-wave bulge; $z < 3$) and disk component ($z \sim 1$) and probably no compact quiescent phase would be observed, i.e., a relatively prominent star-forming disk is always present. In the cartoon, the difference in age between first and second-wave bulges is marked by darker to lighter red colors in the disk galaxies sketched at redshift $z < 1$.

Table 2. Median physical properties of bulges and disks at redshift $0.14 < z \leq 1$.

Type	$\log(M_\star)$	$\bar{t}_M$	$\bar{z}_M$	z_{10}	z_{90}	τ	R_e	$\log(\Sigma_{1.5})$
	($M_\odot$)	(Gyr)				(Myr)	(kpc)	($M_\odot$ kpc$^{-1.5}$)
(1)	(2)	(3)	(4)	(5)	(6)	(7)	(8)	(9)
bulges	$10.5^{+0.3}_{-0.5}$	$2.7^{+3.9}_{-1.6}$	$1.6^{+4.6}_{-0.7}$	$2.0^{+6.8}_{-1.0}$	$1.3^{+3.4}_{-0.6}$	210^{+480}_{-10}	$1.0^{+0.9}_{-0.4}$	$10.4^{+0.5}_{-0.6}$
first-wave bulges	$10.8^{+0.2}_{-0.3}$	$6.5^{+1.5}_{-1.4}$	$6.2^{+1.5}_{-1.7}$	$8.8^{+3.9}_{-2.9}$	$4.7^{+0.7}_{-1.2}$	200^{+20}_{-10}	$1.3^{+0.8}_{-0.6}$	$10.6^{+0.4}_{-0.4}$
second-wave bulges	$10.3^{+0.4}_{-0.5}$	$1.7^{+2.0}_{-0.8}$	$1.3^{+0.6}_{-0.6}$	$1.4^{+1.9}_{-0.6}$	$1.1^{+0.4}_{-0.4}$	210^{+790}_{-10}	$1.0^{+0.8}_{-0.4}$	$10.2^{+0.5}_{-0.4}$
bulges older than disks	$10.6^{+0.3}_{-0.5}$	$4.5^{+2.7}_{-2.8}$	$2.3^{+4.5}_{-1.0}$	$4.0^{+6.2}_{-2.6}$	$1.7^{+3.3}_{-0.6}$	210^{+480}_{-10}	$1.1^{+0.9}_{-0.4}$	$10.5^{+0.5}_{-0.6}$
bulges coeval of disks	$10.4^{+0.1}_{-0.2}$	$1.4^{+1.9}_{-0.6}$	$1.1^{+0.4}_{-0.4}$	$1.2^{+0.4}_{-0.4}$	$1.0^{+0.3}_{-0.4}$	230^{+80}_{-20}	$1.0^{+0.4}_{-0.2}$	$10.3^{+0.3}_{-0.4}$
bulges younger than disks	$10.1^{+0.2}_{-0.5}$	$1.1^{+0.4}_{-1.0}$	$0.8^{+0.5}_{-0.2}$	$0.9^{+0.6}_{-0.2}$	$0.8^{+0.4}_{-0.3}$	200^{+510}_{-10}	$0.7^{+0.7}_{-0.3}$	$10.1^{+0.5}_{-0.3}$
disks	$10.2^{+0.4}_{-0.6}$	$1.2^{+1.6}_{-0.9}$	$1.0^{+0.6}_{-0.3}$	$1.0^{+1.7}_{-0.4}$	$0.9^{+0.3}_{-0.3}$	320^{+950}_{-110}	$5.4^{+3.4}_{-2.0}$	$9.1^{+0.4}_{-0.6}$
disks around first-wave bulges	$10.3^{+0.3}_{-0.7}$	$1.3^{+1.8}_{-0.9}$	$0.9^{+0.9}_{-0.4}$	$1.1^{+2.1}_{-0.5}$	$0.8^{+0.4}_{-0.3}$	360^{+610}_{-160}	$6.3^{+3.1}_{-2.5}$	$9.0^{+0.6}_{-0.5}$
disks around second-wave bulges	$10.2^{+0.3}_{-0.5}$	$1.0^{+1.7}_{-0.8}$	$1.0^{+0.6}_{-0.3}$	$1.0^{+1.1}_{-0.2}$	$0.9^{+0.2}_{-0.3}$	320^{+1110}_{-110}	$4.8^{+2.8}_{-1.4}$	$9.1^{+0.4}_{-0.7}$
disks younger than bulges	$10.2^{+0.3}_{-0.6}$	$0.8^{+0.9}_{-0.6}$	$0.9^{+0.4}_{-0.3}$	$1.0^{+0.6}_{-0.3}$	$0.9^{+0.2}_{-0.3}$	260^{+680}_{-60}	$6.0^{+3.1}_{-2.4}$	$9.0^{+0.5}_{-0.5}$
disks coeval of bulges	$10.4^{+0.3}_{-0.6}$	$1.6^{+2.1}_{-0.7}$	$1.2^{+0.3}_{-0.4}$	$1.6^{+1.8}_{-0.7}$	$0.9^{+0.2}_{-0.2}$	750^{+2140}_{-340}	$6.9^{+0.5}_{-3.4}$	$9.2^{+0.6}_{-0.8}$
disks older than bulges	$10.3^{+0.3}_{-0.2}$	$2.9^{+0.9}_{-1.7}$	$1.5^{+1.0}_{-0.6}$	$2.8^{+2.5}_{-1.9}$	$0.9^{+0.4}_{-0.3}$	900^{+550}_{-690}	$3.6^{+1.9}_{-0.6}$	$9.4^{+0.4}_{-0.3}$